CrossMark

Super-critical and sub-critical bifurcations in a reaction-diffusion Schnakenberg model with linear cross-diffusion

G. Gambino[1] · M. C. Lombardo[1] · S. Lupo[1] · M. Sammartino[1]

© Università degli Studi di Napoli "Federico II" 2016

Abstract In this paper the Turing pattern formation mechanism of a two components reaction-diffusion system modeling the Schnakenberg chemical reaction is considered. In Ref. (Madzavamuse et al., J Math Biol 70(4):709–743, 2015) it was shown how the presence of linear cross-diffusion terms favors the destabilization of the constant steady state. We perform the weakly nonlinear multiple scales analysis to derive the equations for the amplitude of the Turing patterns and to show how the cross-diffusion coefficients influence the occurrence of super-critical or sub-critical bifurcations. We present a numerical exploration of far from equilibrium regimes and prove the existence of multistable stationary solutions.

1 Introduction

The aim of this paper is to describe the Turing pattern formation for the following reaction-diffusion system, recently considered in [25]:

✉ M. Sammartino
  marcomarialuigi.sammartino@unipa.it

[1] Department of Mathematics and Computer Science, University of Palermo, Via Archirafi, 34, 90123 Palermo, Italy

$$\frac{\partial u}{\partial t} = D_u \nabla^2 u + D_{uv} \nabla^2 v + \gamma f(u, v),$$

$$\frac{\partial v}{\partial t} = D_v \nabla^2 v + D_{vu} \nabla^2 u + \gamma g(u, v),$$

(1)

where $D_u, D_v > 0$ are the linear diffusion coefficients, D_{uv}, D_{vu} are the cross-diffusion coefficients, and γ is a positive constant describing the relative strength of reaction terms (or, alternatively, the size of the spatial domain and the time scale). The nonlinear kinetics:

$$f(u, v) = k_1 a_1 - k_2 u + k_3 u^2 v,$$
$$g(u, v) = k_4 b_1 - k_3 u^2 v,$$

(2)

describe the Schnakenberg chemical reaction, where all the coefficients $a_1, b_1,$ k_1, k_2, k_3 and k_4 are positive constants. In (1), $u(\mathbf{x}, t)$ and $v(\mathbf{x}, t)$ with $\mathbf{x} \in \mathbb{R}^n$ are the two chemical concentrations. We shall treat the $1D$ case $\Omega = [0, 2\pi]$.

The system is supplemented with initial conditions and Neumann boundary conditions.

Reaction-diffusion systems have been largely employed in literature to predict the occurrence of spatial patterns in different contexts such as biological sciences, geology, industrial process and networks of electrical circuits [2–4,7,8,20,23,27,28]. Recently, cross-diffusion effects have been considered in models where the gradient of the density of one species induces a flux of another species [11,12,24,30,32,33,38]. It has been shown that, for a large class of predator-prey or competitive kinetics without an autocatalytic term, cross-diffusion is the responsible of Turing instability [15,17, 34,35] and favors pattern formation [16,18]. With the introduction of linear cross-diffusion terms in the Schnakenberg model, the destabilization of the constant steady state occurs even if the diffusion constant of the inhibitor is smaller or equal to the diffusion constant of the activator, see [25]. In this paper we investigate the role of the cross-diffusion coefficients in the occurrence of super-critical or sub-critical Turing bifurcations. When the bifurcation is super-critical, the pattern is spatially extended, it is born from zero amplitude and it is subject to further instabilities in large domains, due to the presence of different unstable modes which interact. In contrast, when the Turing bifurcation is sub-critical, the arising spatial structure jumps to a finite amplitude pattern (which corresponds to a large branch amplitude into the bifurcation diagram). Such sub-critical pattern is localized in the spatial domain, and robust to small fluctuations in the bifurcation parameter values [26]. It is therefore important to investigate what is the mechanism which helps the sub-critical Turing instability. Here we will apply the weakly nonlinear analysis (WNL), a nonlinear bifurcation technique based on the method of multiple scales, to derive a reduced description of the near-critical bifurcation structure of the patterns in terms of their amplitude and to distinguish the super-critical and the sub-critical pattern forming region. We have observed that the occurrence of super- or sub-critical instability strictly depends on the distance between the values of the cross-diffusion coefficients in the inhibitor and the activator component.

On the other hand, the WNL theory yields a reliable approximation of the solution only close to the bifurcation threshold but it is not able to capture the far from the equilibrium dynamics. Therefore we numerically investigate the fully nonlinear regimes computing a bifurcation diagram which proves the existence of stationary non-Turing solutions which are bistable with the Turing pattern. The paper is organized as follows: in Sect. 2 we perform the linear stability analysis to find the conditions on the system parameters for the onset of diffusion-driven instability, draw the corresponding Turing instability region and show how cross-diffusion favors the instability occurrence. In Sect. 3 we carry out the WNL analysis, deriving the equations for the amplitude of the pattern both in the super-critical and the sub-critical bifurcation case and pointing out how cross-diffusion coefficients influence the appearance of super-critical or sub-critical bifurcations. In the case of sub-critical bifurcation, we show that the amplitude equation well describes the hysteretic phenomenon which emerges due to the presence of a multiplicity of stable equilibria. Finally, we numerically investigate far from equilibrium regimes, showing the occurrence of multistability between stationary Turing and non-Turing solutions.

2 Turing instability

We consider the following non dimensional form of the system (1):

$$
\frac{\partial u}{\partial t} = \nabla^2 u + d_v \nabla^2 v + \gamma f(u, v),
$$

$$
\frac{\partial v}{\partial t} = d \nabla^2 v + d_u \nabla^2 u + \gamma g(u, v),
$$

where $d = D_v/D_u$ is the ratio of the linear diffusion coefficients, $d_u = D_{vu}/D_u$ and $d_v = D_{uv}/D_u$ are the ratios of the cross-diffusion coefficients and the linear diffusion coefficients, and the reaction term is given by:

$$
\begin{aligned}
f(u, v) &= a - u + u^2 v, \\
g(u, v) &= b - u^2 v.
\end{aligned}
$$

The details of the above given non-dimensionalization can be found in [25]. Linearizing the system (3)–(4) in the neighborhood of its unique positive steady state:

$$
P_0 = (u_0, v_0) = \left(a + b, \frac{b}{(a+b)^2}\right),
$$

one gets:

$$
\dot{\mathbf{w}} = \gamma J(P_0)\mathbf{w} + D^d \nabla^2 \mathbf{w}, \quad \mathbf{w} \equiv \begin{pmatrix} u - u_0 \\ v - v_0 \end{pmatrix},
$$

where:

$$
D^d = \begin{pmatrix} 1 & d_v \\ d_u & d \end{pmatrix} \quad \text{and} \quad J(P_0) = J = \begin{pmatrix} \frac{b-a}{a+b} & (a+b)^2 \\ -\frac{2b}{a+b} & -(a+b)^2 \end{pmatrix}.
$$

We impose that the following condition holds:

$$\det(D^d) = d - d_u d_v > 0, \tag{7}$$

in such a way that the reaction-diffusion system (3) is well posed.

Through linear stability analysis the following dispersion relation is found, which gives the growth rate λ as a function of the wavenumber k:

$$\lambda^2 - t(k^2)\lambda + h(k^2) = 0, \tag{8}$$

where:

$$t(k^2) = \gamma \operatorname{tr} J - k^2(1 + d),$$
$$h(k^2) = \det(D^d)k^4 + \gamma q k^2 + \gamma^2 \det(J), \quad \text{with} \quad q = -J_{11}D_{22}^d - J_{22}D_{11}^d. \tag{9}$$

Being $\det(J) = (a + b)^2 > 0$, in order for the steady state P_0 to be stable to the spatially homogeneous mode $k = 0$, one has to require that $\operatorname{tr}(J) < 0$. The equilibrium loses its stability via Turing bifurcation if $\mathfrak{Re}(\lambda) > 0$ for some $k \neq 0$, which is equivalent to impose $h(k^2) < 0$ for some $k \neq 0$. Since, from (7), $h(k^2)$ is an upward opening parabola (see Fig. 1a), the following two conditions have to be satisfied:

$$q < 0, \tag{10}$$
$$q^2 - 4\det(D^d)\det(J) > 0. \tag{11}$$

As $D_{ii}^d > 0, i = 1, 2$ and $J_{22} < 0$, condition (10) and the expression in (9) for q imply that $J_{11} > 0$ is a necessary condition for Turing instability, which is equivalent to assume $b > a$. Therefore, the Schnakenberg model has to belong to the class of activator-inhibitor system; in particular, being $J_{22} < 0$, $J_{12} > 0$ and $J_{21} < 0$, it is a so called *cross activator-inhibitor* system. The neutral stability Turing boundary corresponds to $h(k^2) = 0$, which has a single minimum (k_c^2, d_c) attained when:

$$k_c^2 = \gamma \sqrt{\frac{\det(J)}{d_c - d_u d_v}}, \tag{12}$$

and, by imposing $q^2 - 4\det(D^d)\det(J) = 0$, the corresponding Turing bifurcation value d_c is obtained as follows:

$$d_c = (\det(J) - J_{12}J_{21} + J_{11} \ (d_v J_{21} + d_u J_{12}))/J_{11}^2$$
$$+ 2\sqrt{\frac{\det(J)(d_v J_{11} - J_{12})(J_{21} - d_u J_{11})}{J_{11}}}. \tag{13}$$

From the above discussion we can state the following theorem that was originally formulated in [25].

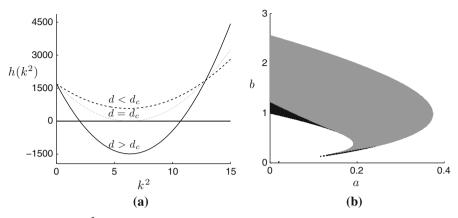**Theorem 1** *The necessary conditions for diffusion driven instability of the system* (3) *are:*

Fig. 1 **a** Plot of $h(k^2)$. **b** Turing instability region in the plane (a, b) is shadowed: in *grey* the super-critical region, in *black* the sub-critical region (see details in Sect. 3). The other parameter values are chosen as $\gamma = 1$, $d = 15$, $d_u = 1$ and $d_v = 1$

(i) $\text{tr}(J) < 0$;
(ii) $q = -J_{11}D_{22}^d - J_{22}D_{11}^d < 0$;
(iii) $J_{11} > 0$;
(iv) $q^2 - 4\det(D^d)\det(J) > 0$.

Therefore at $d = d_c$ as defined in (13), stationary spatially periodic solution whose wavenumber k_c given in (12), bifurcate from the homogeneous steady state. In Fig. 1b, the Turing instability region, i.e. the region in the parameter space where the conditions (i)–(iv) are satisfied, is shown in the section (a, b) of the parameter space. The parameter γ plays no role in the characterization of the Turing instability region, as the conditions (i)–(iv) do not depend on its value. For $d > d_c$ the system admits a finite k pattern-forming stationary instability, see Fig. 1a. However, since the spatial eigenmodes allowed by the boundary conditions form a discrete set, it could happen that none of the admissible modes has positive growth factor. To guarantee the emergence of spatial patterns at least one of the modes allowed by the boundary conditions must fall within the interval of instability $[k_1^2; k_2^2]$, where k_1 and k_2 are the roots of $h(k^2)$ and are proportional to γ. Recalling that the modes allowed by the no-flux boundary conditions on the spatial domain $[0, 2\pi]$ are of the form $k = n/2$ with $n \in \mathbb{N}$, one can therefore state the following theorem.

Theorem 2 *Let k_1 and k_2 be the roots of $h(k^2)$, then the formation of the pattern occurs if*

- *conditions* (i)–(iv) *of Theorem* 1 *are satisfied;*
- γ *is large enough so that there exists at least one integer $\bar{n}$ such that $k_1 \leq \bar{n}/2 \leq k_2$.*

In absence of cross-diffusion, condition (ii) of Theorem 1 reduces to $d J_{11} + J_{22} > 0$. This condition, together with (i), leads to $d > -\frac{J_{22}}{J_{11}} > 1$, therefore the diffusion coefficients of the two species can not be equal and the inhibitor v must diffuse faster than the activator u. This does not hold true in presence of the cross diffusive coefficients (as it has been observed in [25]).

Moreover, d_c in (13) must be a real number, i.e. $\det(J)(d_v J_{11} - J_{12})(J_{21} - d_u J_{11})$ has to be non-negative. Being $\det(J) > 0$, the cross-diffusion coefficients d_u and d_v should be chosen in one of the following two sets:

$$S_1 = \left\{ (d_u, d_v) : d_u \geq \frac{J_{21}}{J_{11}}, d_v \leq \frac{J_{12}}{J_{11}} \right\}, \quad S_2 = \left\{ (d_u, d_v) : d_u \leq \frac{J_{21}}{J_{11}}, d_v \geq \frac{J_{12}}{J_{11}} \right\}.$$

If $(d_u, d_v) \in S_2$, then $d_u \leq J_{21}/J_{11} < 0$. The negative cross-diffusion, discussed e.g. in [10,31], represents an unnatural tendency of a species to move against the concentration gradient of the other species and it is quite rare. Therefore, in what follows, the cross-diffusion coefficients will be chosen in S_1.

Let us now investigate the cases in which d_u or d_v is equal to zero.

If $d_u = 0$ the derivative of d_c with respect to d_v computed at $d_u = 0$, i.e. in absence of cross-diffusion, is given by:

$$\frac{\partial d_c}{\partial d_v}\Big|_{d_u=0} = -\frac{2b}{b-a} \left[1 + \frac{(a+b)^2}{\sqrt{d_v(b-a) + (a+b)^3}} \right]$$

and it is always negative. Therefore, the threshold value d_c decreases as d_v increases and, correspondingly, the Turing instability region becomes larger. Notice, however, that the Turing instability does not arise if the cross-diffusion coefficient becomes too large, i.e. exceeds $J_{12}/J_{11} = (a+b)^3/b - a$. If $d_v = 0$, the effect is opposite. In fact, the derivative of d_c with respect to d_u, computed at $d_v = 0$:

$$\frac{\partial d_c}{\partial d_u}\Big|_{d_v=0} = \frac{(a+b)^3}{b-a} \left[1 + \frac{b-a}{(a+b)\sqrt{2b + d_u(b-a)}} \right]$$

is positive. Hence, the bifurcation value d_c increases as d_u increases and the corresponding Turing instability region becomes smaller. In Fig. 2 we plot the bifurcation
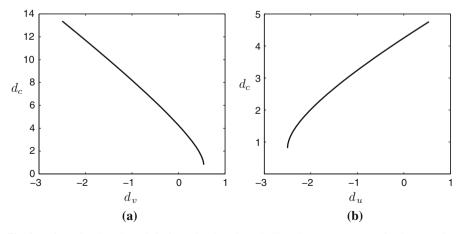

Fig. 2 **a** d_c vs d_v when $d_u = 0$; **b** d_c vs d_u when $d_v = 0$. The other parameters are fixed as $a = 0.1$, $b = 0.5$ and $\gamma = 1$
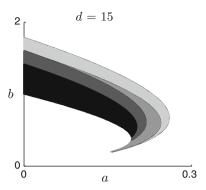
Fig. 3 Turing region in the parameter space (a, b) for $d = 15$. A *grey-scale* is used to show the following inclusion chain of Turing regions: the Turing region with $d_u = 1$ and $d_v = 0$ (in *dark*) is the smallest one, it is included in the Turing region in absence of cross-diffusion (in *dark grey*), which in turn is included in the Turing region with $d_u = 1$ and $d_v = 1$ (in *light grey*), which is finally included in that one with $d_u = 0$ and $d_v = 1$ (in *lighter grey*)

value d_c respectively versus d_v and d_u, choosing $a = 0.1$ and $b = 0.5$. The minimum value of the Turing bifurcation parameter d_c attained at the boundaries of the set $S_1 \{(d_u, d_v) : d_u \geq -2.5, d_v \leq 0.54\}$ is 0.81, i.e. a value less than 1, which means that, in presence of cross-diffusion, Turing instability occurs also not assuming short range activation-long range inhibition. Our results are in agreement with [25]. We can conclude, in agreement with the results in [25], that cross-diffusion in the inhibitor component only ($d_v = 0$) produces the smallest parameter space, cross-diffusion in the activator component only ($d_u = 0$) gives the biggest parameter space and it contains the former one. Moreover, the Turing region corresponding to the reaction-diffusion system without cross-diffusion ($d_u = 0$ and $d_v = 0$) is a subspace of the Turing region of the reaction-diffusion system with cross-diffusion in both u and v. These behaviours are summarized in Fig. 3.

3 WNL analysis and pattern formation

Once the conditions on the system parameters for the onset of diffusion driven instability have been obtained, we perform a WNL analysis to derive a reduced description of the near-critical bifurcation structure of the patterns in terms of their amplitude. Defining the control parameter as the dimensionless distance from the threshold $\varepsilon^2 = (d - d_c)/d_c$, the solution of the original system (3) is written as a weakly nonlinear expansion in ε:

$$\mathbf{w} = \varepsilon \mathbf{w}_1 + \varepsilon^2 \mathbf{w}_2 + \varepsilon^3 \mathbf{w}_3 + \cdots , \tag{14}$$

Close to the bifurcation the amplitude of the pattern evolves on a slow temporal scale, therefore we separate the fast time t and slow time T:

$$\frac{\partial}{\partial t} = \varepsilon \frac{\partial}{\partial T_1} + \varepsilon^2 \frac{\partial}{\partial T_2} + \varepsilon^3 \frac{\partial}{\partial T_3} \cdots . \tag{15}$$

Moreover, we expand the bifurcation parameter d as follows:

$$d = d_c + \varepsilon d^{(1)} + \varepsilon^2 d^{(2)} + \varepsilon^3 d^{(3)} + \cdots . \tag{16}$$

Upon substitution of the expansions (14)–(16) into (3), we collect the terms at each order in ε obtaining the following sequence of equations for the $\mathbf{w}_i$: $O(\varepsilon)$:

$$\mathcal{L}^{d_c} \mathbf{w}_1 = \mathbf{0}, \tag{17}$$

$O(\varepsilon^2)$:

$$\mathcal{L}^{d_c} \mathbf{w}_2 = \mathbf{F}, \tag{18}$$

$O(\varepsilon^3)$:

$$\mathcal{L}^{d_c} \mathbf{w}_3 = \mathbf{G}, \tag{19}$$

where $\mathcal{L}^{d_c} = J + D^{d_c} \nabla^2$ and:

$$\mathbf{F} = \frac{\partial \mathbf{w}_1}{\partial T_1} - \begin{pmatrix} 0 & 0 \\ 0 & d^{(1)} \end{pmatrix} \nabla^2 \mathbf{w}_1 - \gamma \begin{pmatrix} 2(a+b)u_1 v_1 + \frac{b}{(a+b)^2} u_1^2 \\ -2(a+b)u_1 v_1 - \frac{b}{(a+b)^2} u_1^2 \end{pmatrix},$$

$$\mathbf{G} = \frac{\partial \mathbf{w}_1}{\partial T_2} + \frac{\partial \mathbf{w}_2}{\partial T_1} - \begin{pmatrix} 0 & 0 \\ 0 & d^{(1)} \end{pmatrix} \nabla^2 \mathbf{w}_2 - \begin{pmatrix} 0 & 0 \\ 0 & d^{(2)} \end{pmatrix} \nabla^2 \mathbf{w}_1 - \gamma \begin{pmatrix} u_1^2 v_1 \\ -u_1^2 v_1 \end{pmatrix}$$

$$- \gamma \begin{pmatrix} \frac{2b}{(a+b)^2} u_1 + 2(a+b)v_1 & 2(a+b)u_1 \\ -\frac{2b}{(a+b)^2} u_1 - 2(a+b)v_1 & -2(a+b)u_1 \end{pmatrix} \mathbf{w}_2.$$

The solution to the linear problem (17), which satisfies the Neumann boundary conditions, is:

$$\mathbf{w}_1 = A(T_1, T_2, \ldots) \mathbf{r} \cos(\bar{k}_c x), \quad \text{with} \quad \mathbf{r} \in \text{Ker}(J - \bar{k}_c^2 D^{d_c}), \tag{20}$$

where the amplitude of the pattern $A(T_1, T_2, \ldots)$ is still arbitrary at this level, $\bar{k}_c$ is the first unstable admissible mode and the vector $\mathbf{r}$, defined up to a constant, is normalized as follows:

$$\mathbf{r} = \begin{pmatrix} 1 \\ M \end{pmatrix} \quad \text{with} \quad M = \frac{-\bar{k}_c^2 - \gamma \frac{2b}{a+b}}{\gamma (a+b)^2 + \bar{k}_c^2 d_c}. \tag{21}$$

Substituting the solution (20) in (18), we assume $T_1 = 0$ and $d^{(1)} = 0$ in such a way that the vector $\mathbf{F}$ is automatically orthogonal to the kernel of the adjoint of $\mathcal{L}^{d_c}$. Hence the solution of (18) can be straightforwardly computed and, once substituted into (19), yields the following expression for the source term $\mathbf{G}$:

$$\mathbf{G} = \left(\frac{dA}{dT} \mathbf{r} + A \mathbf{G}_1^{(1)} + A^3 \mathbf{G}_1^{(3)} \right) \cos(\bar{k}_c x) + \mathbf{G}^*, \tag{22}$$

where $T = T_2$ and the vectors $\mathbf{G}_1^j$, $j = 1, 3$ and $\mathbf{G}^*$ (containing only orthogonal terms to the kernel of the adjoint of $\mathcal{L}^{d_c}$) are computed in terms of the parameters of the original system (3) as follows:

$$\mathbf{G}_1^{(1)} = \begin{pmatrix} 0 \\ d^{(2)} k_c^2 M \end{pmatrix}, \qquad \mathbf{G}_1^{(3)} = -\gamma \bar{\mathbf{G}} \left(\mathbf{w}_{20} + \frac{1}{2} \mathbf{w}_{22} \right) - \frac{3}{4} \gamma M \begin{bmatrix} 1 \\ -1 \end{bmatrix},$$

$$\mathbf{G}^* = -\frac{1}{2} \gamma \bar{\mathbf{G}} \mathbf{w}_{22} - \frac{1}{4} \gamma M \begin{bmatrix} 1 \\ -1 \end{bmatrix}, \quad \bar{\mathbf{G}} = \begin{pmatrix} \frac{2b}{(a+b)^2} + 2(a+b)M & 2(a+b) \\ -\frac{2b}{(a+b)^2} - 2(a+b)M & -2(a+b) \end{pmatrix}.$$

Upon setting:

$$\sigma = -\frac{\left\langle \mathbf{G}_1^{(1)}, \boldsymbol{\psi} \right\rangle}{\langle \mathbf{r}, \boldsymbol{\psi} \rangle}, \qquad L = \frac{\left\langle \mathbf{G}_1^{(3)}, \boldsymbol{\psi} \right\rangle}{\langle \mathbf{r}, \boldsymbol{\psi} \rangle}, \tag{23}$$

where $\boldsymbol{\psi} \in Ker\left\{ \left(J - \bar{k}_c^2 D^{d_c} \right)^\dagger \right\}$, the solvability condition $\langle \mathbf{G}, \boldsymbol{\psi} \rangle = 0$ for the Eq. (22), leads to the following Stuart–Landau equation:

$$\frac{dA}{dT} = \sigma A - L A^3. \tag{24}$$

The stability behavior of the Stuart–Landau equation (24) and consequently the pattern formation for the model system is dependent upon the sign of the Landau constant L. When $L > 0$ the WNL analysis provides an asymptotic solution for the reaction-diffusion system (3):

Theorem 3 (*Super-critical bifurcation*) *Assume that:*

1. $\varepsilon^2 = (d - d_c)/d_c$ *is small enough so that the uniform steady state* (u_0, v_0) *is unstable to modes corresponding only to the eigenvalue* $\bar{k}_c$;
2. *the Landau coefficient L in* (23) *is greater than zero.*

Then the emerging solution of the reaction-diffusion system (3) *is given by:*

$$\mathbf{w} = \varepsilon \mathbf{r} A_\infty \cos(\bar{k}_c x) + O(\varepsilon^2), \tag{25}$$

where $A_\infty = \sqrt{\sigma/L}$ *is the stable stationary state of the Stuart–Landau equation* (24) *and* $\mathbf{r} \in Ker(J - \bar{k}_c^2 D^{d_c})$.

We pick the system parameters in the super-critical parameter region shown in Fig. 1b and in such a way that, in the domain $[0, 2\pi]$ the only admitted discrete unstable mode is $\bar{k}_c = 2.5$. Comparing the asymptotic solution predicted by the WNL analysis and the numerical solution of the system (3) computed with a spectral numerical code starting from a random periodic perturbation of the constant state, we obtain a very good agreement, see Fig. 4a. In particular, in all the performed numerical experiments, we have verified that the distance, evaluated in the L^1 norm, between the WNL approximation (25) and the numerical solution of the system is $O(\varepsilon^3)$.

For some choices of the system parameters, the Landau coefficient L has a negative value. In these cases a sub-critical bifurcation occurs and Eq. (24) is not able to predict the amplitude of the pattern. In order to capture the evolution of pattern amplitude we push the WNL analysis up to $O(\varepsilon^5)$, obtaining the following quintic Stuart–Landau equation for the amplitude A:
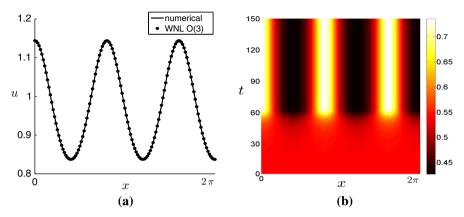
Fig. 4 **a** Comparison between the WNL approximated solution (*dotted line*) and the numerical solution of the reaction-diffusion system (3) (*solid line*). **b** Pattern evolution in the space-time plane. Here the parameters are chosen in the super-critical region: $a = 0.34$ and $b = 0.64$, $d_u = 1$, $dv = 1$, $\gamma = 42$ so that $d_c = 43.9864$ and $\bar{k}_c = 2.5$; $d = d_c(1 + \varepsilon^2)$ with $\varepsilon^2 = 0.04$

$$\frac{dA}{dT} = \bar{\sigma} A - \bar{L} A^3 + \bar{R} A^5. \tag{26}$$

The details of the analysis and the expressions of the coefficients of the above equation are given in "Appendix". The results can be summarized as follows:

Proposition 1 (WNL analysis results in the sub-critical case)
   Assume that the hypotheses (1) *and* (2) *of Theorem* 3 *hold and that*

(3) *the Landau coefficient L into* (24) *is negative;*
(4) *the coefficient $\bar{R}$ into* (26) *is positive.*

   Then the emerging solution of the reaction-diffusion system (3) *is given by:*

$$\mathbf{w} = \varepsilon \mathbf{r} A_\infty \cos(k_c x) + O(\varepsilon), \tag{27}$$

where A_∞ is a stable stationary state of the quintic Stuart–Landau equation (26).

The emerging pattern in the sub-critical case is an $O(1)$ perturbation of the equilibrium (in fact the amplitude A is order ε^{-1}, see e.g. [17]). This is of course a contradiction with the basic assumption of the perturbation scheme, so that, in the sub-critical case, the expected solution by the WNL analysis may fail to capture the quantitative features of the emerging structures. Nevertheless, our simulation in Fig. 5 show that such an expansion gives a reasonable qualitative insight on the pattern close to the sub-critical threshold.

In order to detect how too cumbersome and, therefore, are here omitted the cross-diffusion coefficients influence the occurrence of supercritical or sub-critical bifurcation, we represent the Turing super- and sub-critical regions for suitable values of d_u and d_v. In Fig. 6a we observe that, when $d_u < d_v$ the Turing instability occurs through a supercritical bifurcation for most of the values. The sub-critical region
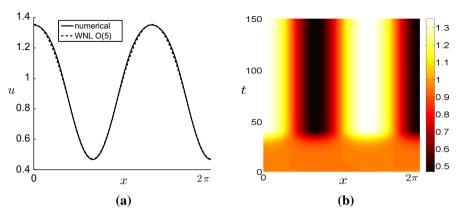
(a)   **(b)**

Fig. 5 **a** Comparison between the weakly nonlinear solution (*solid line*) and the numerical solution of (3). **b** Pattern evolution in the space-time plane. The parameters are chosen as $a = 0.1$, $b = 0.85$, $\gamma = 5$, $d_u = 5$, $d_v = 1$, so that $d_c = 9.9431$ and $\bar{k}_c = 1.5$; $d = d_c(1 + \varepsilon^2)$ with $\varepsilon^2 = 0.15$. This pattern corresponds, in the numerically computed bifurcation diagram Fig. 8, to the point labeled by $*$
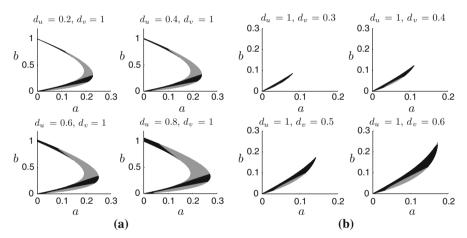

(a)   **(b)**

Fig. 6 Turing instability regions: in *grey* the super-critical region and in *black* the sub-critical region. The parameters are chosen as $d = 1$ and $\gamma = 1$

increases as the distance between d_u and d_v decreases. When $d_u > d_v$ the behaviour is opposite, as shown in Fig. 6b. In fact, the Turing instability occurs through a sub-critical bifurcation for most of the values and the supercritical region arises in correspondence of a decreasing of the distance between d_u and d_v.

3.1 Sub-critical bifurcation and bistability

The Eq. (26) is also able to describe the interesting phenomenon of hysteresis. In the bifurcation diagram predicted by the WNL analysis, shown in Fig. 7a, one can see that two qualitatively different stable states coexist when $d_s < d < d_c$. The hysteresis cycle in Fig. 7b shows that, starting with a value of the parameter above d_c, the
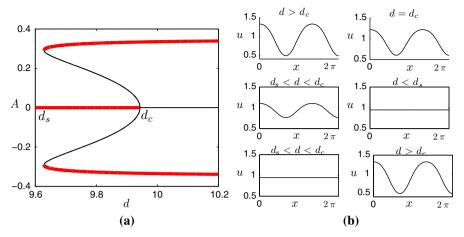
(a)

(b)

Fig. 7 **a** The bifurcation diagram predicted by WNL analysis in the sub-critical case (the stable branches are drawn with *red thick line*, the unstable ones with *black thin line*). **b** A hysteresis cycle and the corresponding pattern evolution in the sub-critical case. As d varies, the fixed values of the other parameters are the same as in Fig. 5
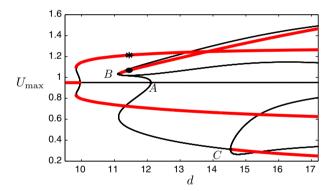

Fig. 8 Numerically calculated bifurcation diagram: the stable branches are drawn in *red thick line*, the unstable ones in *black thin line*. As d varies, the fixed values of the other parameters are the same as in Fig. 5. The patterns corresponding to the points marked by *asterisk* and *bullet* are shown in Figs. 5 and 9, respectively

solution stabilizes to a pattern corresponding to the stable large amplitude branch of the bifurcation diagram. Decreasing d below d_c the pattern does not disappear, as the stable amplitude solution persists on the upper branch. Still decreasing d below d_s the pattern disappears, as the amplitude solution jumps to the constant steady state. The formation of the pattern is again obtained only increasing the parameter d above d_c.

To investigate the system behavior far from equilibrium, we computed the corresponding bifurcation diagram as the parameter d is varied in the interval $d \in [9, 18]$, using the numerical continuation software AUTO. In Fig. 8 the numerically calculated bifurcation diagram of the point x_{max} where the species u attains its maximum U_{max} on the large amplitude branch is shown.
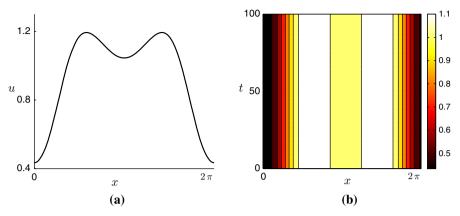
Fig. 9 Stationary solution far from the equilibrium. **a** Profile of the solution. **b** Pattern evolution in the space-time plane. The parameters are chosen as in Fig. 5 and $d = 11.45$

Near the threshold d_c, the bifurcation diagram predicted using the WNL analysis qualitative agrees with the one numerically computed. As d increases from d_c, the homogeneous unstable steady state undergoes to a bifurcation at $d_A \simeq 12.11$, at the point labeled by A in Fig. 8, where two different unstable branches emerge. Secondary bifurcations occur on both branches, at the points B (with $d_B \simeq 11.12$) and C (with $d_C \simeq 14.52$), respectively, which give rise to stable stationary patterns, whose existence cannot be predicted by the weakly nonlinear expansion. The pattern computed on the upper branch for $d \simeq 11.45$ (at the point labeled by a solid bullet in Fig. 8) is shown in Fig. 9. It is a far-from-equilibrium stationary solution which is different, for amplitude and form, from the expected pattern on the basis on the WNL theory for the same value of the parameter d, which has been depicted in Fig. 5. Its analytical investigation is a subject of great interest (see e.g. [21,22]) and will be the object of a forthcoming paper. Therefore, for a fixed value of the bifurcation parameter, bistability occurs and two different stable patterns coexist when $d > d_B$.

The pattern solution computed on the lower stable branch arising from the point C differs from the corresponding one on the upper branch only for a phase shift and, therefore, is not shown here.

4 Conclusions

In this paper we have investigated the Turing instability induced by linear cross-diffusion for the Schnakenberg reaction-diffusion system. By performing a WNL analysis, we have predicted the amplitude of the pattern near the threshold and we have determined the super- and the sub-critical instability regions whose extent depends on the distance between the values of the cross diffusion coefficients. Multiple branches of stable solutions are also observed leading to hysteresis next to the threshold and far from the equilibrium.

Other aspects of the problem could be examined. For example it is well known how the interaction between the Turing and the Hopf instability mechanisms, can give rise to

non-stationary patterns [37]; the Schnakenberg kinetics supports the Hopf bifurcation and one should analyze the parameter region where spatio-temporal structures could emerge as the result of this codimension-2 bifurcation. Moreover it has been recently shown [1,34] how oscillatory dynamics can also be induced, away from threshold, by strong nonlinear mechanisms, leading also to the onset of chaotic phenomena [5,6]: one could ask whether this behavior is supported by the system considered in the present paper. We mention that a typical far from the equilibrium phenomenon is the appearance of localized structures like spots or mesa patterns that could be rigorously constructed though matched asymptotic procedures. We also report that in some of our numerical tests we have seen the appearance of metastable structure that, either disappear giving rise to different patterns or decay to equilibrium; it would be of interest to study these long time behaviors via the techniques used in [29]; or to investigate how the coherent structures supported by the Schnakenberg system are modified by the presence of non-autonomous kinetic terms of the form considered in [9]. The design of suitable finite-dimensional controls of feedback or adaptive type [13,14,19,36] to control the complex behavior supported by our system would also deserve some attention.

Appendix: The quintic Stuart–Landau equation

Taking into account that (24) still holds for the amplitude A (although now the derivative with respect to T is a partial derivative), the solvability condition $\langle \mathbf{G}, \psi \rangle = 0$ for (19) is satisfied and the solution is:

$$\mathbf{w}_3 = \left(A \mathbf{w}_{31} + A^3 \mathbf{w}_{32} \right) \cos \left(k_c x \right) + A^3 \mathbf{w}_{33} \cos \left(3 k_c x \right), \tag{28}$$

where the expression for the vectors $\mathbf{w}_{3i}, i = 1, 2, 3$ can be computed solving the following linear systems:

$$L_1 \mathbf{w}_{31} = \sigma \mathbf{r} + \mathbf{G}_1^{(1)}, \quad L_2 \mathbf{w}_{32} = -L \mathbf{r} + \mathbf{G}_1^{(3)}, \quad L_3 \mathbf{w}_{33} = \mathbf{G}_3,$$

where we have defined $L_i = \Gamma J - i^2 k_c^2 D^{d_c}$.

At $O(\varepsilon^4)$ the resulting equation is $\mathcal{L}^{d_c} \mathbf{w}_3 = \mathbf{H}$, where:

$$\mathbf{H} = 2A \frac{\partial A}{\partial T_2} \mathbf{w}_{20} + A^2 \mathbf{H}_0^{(2)} + A^4 \mathbf{H}_0^{(4)} + \left(2A \frac{\partial A}{\partial T} \mathbf{w}_{22} + A^2 \mathbf{H}_2^{(2)} + A^4 \mathbf{H}_2^{(4)} \right) \cos(2\bar{k}_c x)$$

$$+ A^4 \mathbf{H}_4^{(4)} \cos(4\bar{k}_c x),$$

and:

$$\mathbf{H}_0^{(2)} = \frac{1}{2}\gamma \begin{pmatrix} \frac{2b}{(a+b)^2} + 2(a+b)M & 2(a+b) \\ -\frac{2b}{(a+b)^2} - 2(a+b)M & -2(a+b) \end{pmatrix} \mathbf{w}_{31},$$

$$\mathbf{H}_0^{(4)} = \frac{1}{2}\gamma \begin{pmatrix} \frac{2b}{(a+b)^2} + 2(a+b)M & 2(a+b) \\ -\frac{2b}{(a+b)^2} - 2(a+b)M & -2(a+b) \end{pmatrix} \mathbf{w}_{32}$$

$$+ \gamma \begin{pmatrix} \frac{b}{(a+b)^2}\mathbf{w}_{20}(1) + 2(a+b)\mathbf{w}_{20}(2) + M & \frac{1}{2} \\ -\frac{b}{(a+b)^2}\mathbf{w}_{20}(1) - 2(a+b)\mathbf{w}_{20}(2) - M & -\frac{1}{2} \end{pmatrix} \mathbf{w}_{20}$$

$$+ \frac{1}{2}\gamma \begin{pmatrix} \frac{b}{(a+b)^2}\mathbf{w}_{22}(1) + 2(a+b)\mathbf{w}_{22}(2) + M & \frac{1}{2} \\ -\frac{b}{(a+b)^2}\mathbf{w}_{22}(1) - 2(a+b)\mathbf{w}_{22}(2) - M & -\frac{1}{2} \end{pmatrix} \mathbf{w}_{22}$$

$$\mathbf{H}_2^{(2)} = \begin{pmatrix} 0 & 0 \\ 0 & 4d^{(2)}k_c^2 \end{pmatrix} \mathbf{w}_{22} + \frac{1}{2}\gamma \begin{pmatrix} \frac{2b}{(a+b)^2} + 2(a+b)M & 2(a+b) \\ -\frac{2b}{(a+b)^2} - 2(a+b)M & -2(a+b) \end{pmatrix} \mathbf{w}_{31},$$

$$\mathbf{H}_2^{(4)} = \frac{1}{2}\gamma \begin{pmatrix} \frac{2b}{(a+b)^2} + 2(a+b)M & 2(a+b) \\ -\frac{2b}{(a+b)^2} - 2(a+b)M & -2(a+b) \end{pmatrix} (\mathbf{w}_{32} + \mathbf{w}_{33})$$

$$+ \gamma \begin{pmatrix} \frac{b}{(a+b)^2}\mathbf{w}_{20}(1) + 2(a+b)\mathbf{w}_{20}(2) + M & \frac{1}{2} \\ -\frac{b}{(a+b)^2}\mathbf{w}_{20}(1) - 2(a+b)\mathbf{w}_{20}(2) - M & -\frac{1}{2} \end{pmatrix} \mathbf{w}_{22}$$

$$+ \gamma \begin{pmatrix} \frac{b}{(a+b)^2}\mathbf{w}_{22}(1) + 2(a+b)\mathbf{w}_{22}(2) + M & \frac{1}{2} \\ -\frac{b}{(a+b)^2}\mathbf{w}_{22}(1) - 2(a+b)\mathbf{w}_{22}(2) - M & -\frac{1}{2} \end{pmatrix} \mathbf{w}_{20},$$

$$\mathbf{H}_4^{(4)} = \frac{1}{2}\gamma \begin{pmatrix} \frac{2b}{(a+b)^2} + 2(a+b)M & 2(a+b) \\ -\frac{2b}{(a+b)^2} - 2(a+b)M & -2(a+b) \end{pmatrix} \mathbf{w}_{33}$$

$$+ \frac{1}{2}\gamma \begin{pmatrix} \frac{b}{(a+b)^2}\mathbf{w}_{22}(1) + 2(a+b)\mathbf{w}_{22}(2) + M & \frac{1}{2} \\ -\frac{b}{(a+b)^2}\mathbf{w}_{22}(1) - 2(a+b)\mathbf{w}_{22}(2) - M & -\frac{1}{2} \end{pmatrix} \mathbf{w}_{22}.$$

The solvability condition for is automatically satisfied and the solution is:

$$\mathbf{w}_4 = A^2\mathbf{w}_{40} + A^4\mathbf{w}_{41} + \left(A^2\mathbf{w}_{42} + A^4\mathbf{w}_{43}\right)\cos(2k_cx) + A^4\mathbf{w}_{44}\cos(4k_cx), \quad (29)$$

where the vector $\mathbf{w}_{4i}$, $i = 1, \ldots, 4$, are the solutions of the following linear systems:

$$\Gamma K \mathbf{w}_{40} = 2\sigma \mathbf{w}_{20} + \mathbf{H}_0^{(2)}, \quad \Gamma K \mathbf{w}_{41} = -2L\mathbf{w}_{20} + \mathbf{H}_0^{(4)},$$
$$L_2\mathbf{w}_{42} = 2\sigma \mathbf{w}_{22} + \mathbf{H}_2^{(2)}, \quad L_3\mathbf{w}_{43} = -2L\mathbf{w}_{22} + \mathbf{H}_2^{(4)}, \quad L_4\mathbf{w}_{44} = \mathbf{H}_4.$$

At $O(\varepsilon^5)$ the resulting equation is $\mathcal{L}^{d_c}\mathbf{w}_3 = \mathbf{P}$, where:

$$\mathbf{P} = \left(\frac{\partial A}{\partial T_4}\mathbf{r} + \frac{\partial A}{\partial T_2}\mathbf{w}_{31} + 3A^2\frac{\partial A}{\partial T_2}\mathbf{w}_{32} + A\mathbf{P}_1^{(1)} + A^3\mathbf{P}_1^{(3)} + A^5\mathbf{P}_1^{(5)}\right)\cos(\bar{k}_c x) \tag{30}$$

$$+ \left(3A^2\frac{\partial A}{\partial T_2}\mathbf{w}_{33} + A^3\mathbf{P}_3^{(3)} + A^5\mathbf{P}_3^{(5)}\right)\cos(3\bar{k}_c x) + A^5\mathbf{P}_5^{(5)}\cos(5\bar{k}_c x), \tag{31}$$

and:

$$\mathbf{P}_1^{(1)} = \begin{pmatrix} 0 & 0 \\ 0 & d^{(2)}k_c^2 \end{pmatrix}\mathbf{w}_{31} + \begin{pmatrix} 0 \\ d^{(4)}k_c^2 M \end{pmatrix},$$

$$\mathbf{P}_1^{(3)} = \begin{pmatrix} 0 & 0 \\ 0 & d^{(2)}k_c^2 \end{pmatrix}\mathbf{w}_{32} - \gamma\begin{pmatrix} \frac{2b}{(a+b)^2} + 2(a+b)M & 2(a+b) \\ -\frac{2b}{(a+b)^2} - 2(a+b)M & -2(a+b) \end{pmatrix}\left(\mathbf{w}_{40} + \frac{1}{2}\mathbf{w}_{42}\right)$$

$$- \gamma\begin{pmatrix} \frac{2b}{(a+b)^2}\mathbf{w}_{20}(1) + 2(a+b)\mathbf{w}_{20}(2) & 2(a+b)\mathbf{w}_{20}(1) + \frac{1}{2} \\ -\frac{2b}{(a+b)^2}\mathbf{w}_{20}(1) - 2(a+b)\mathbf{w}_{20}(2) & -2(a+b)\mathbf{w}_{20}(1) - \frac{1}{2} \end{pmatrix}\mathbf{w}_{31}$$

$$- \frac{1}{2}\gamma\begin{pmatrix} \frac{2b}{(a+b)^2}\mathbf{w}_{22}(1) + 2(a+b)\mathbf{w}_{22}(2) & 2(a+b)\mathbf{w}_{22}(1) + \frac{1}{2} \\ -\frac{2b}{(a+b)^2}\mathbf{w}_{22}(1) - 2(a+b)\mathbf{w}_{22}(2) & -2(a+b)\mathbf{w}_{22}(1) - \frac{1}{2} \end{pmatrix}\mathbf{w}_{31},$$

$$\mathbf{P}_1^{(5)} = -\gamma\begin{pmatrix} \frac{2b}{(a+b)^2} + 2(a+b)M & 2(a+b) \\ -\frac{2b}{(a+b)^2} - 2(a+b)M & -2(a+b) \end{pmatrix}\left(\mathbf{w}_{41} + \frac{1}{2}\mathbf{w}_{43}\right)$$

$$- \gamma\begin{pmatrix} \frac{2b}{(a+b)^2}\mathbf{w}_{20}(1) + 2(a+b)\mathbf{w}_{20}(2) & 2(a+b)\mathbf{w}_{20}(1) + \frac{1}{2} \\ -\frac{2b}{(a+b)^2}\mathbf{w}_{20}(1) - 2(a+b)\mathbf{w}_{20}(2) & -2(a+b)\mathbf{w}_{20}(1) - \frac{1}{2} \end{pmatrix}\mathbf{w}_{32}$$

$$- \gamma\begin{pmatrix} \frac{2b}{(a+b)^2}\mathbf{w}_{20}(1) + 2(a+b)\mathbf{w}_{20}(2) & 2(a+b)\mathbf{w}_{20}(1) + \frac{1}{2} \\ -\frac{2b}{(a+b)^2}\mathbf{w}_{20}(1) - 2(a+b)\mathbf{w}_{20}(2) & -2(a+b)\mathbf{w}_{20}(1) - \frac{1}{2} \end{pmatrix}(\mathbf{w}_{32}+\mathbf{w}_{33})$$

$$- \gamma\begin{pmatrix} \left(\mathbf{w}_{20}(1) + \frac{1}{2}\mathbf{w}_{22}(1)\right)M & 2\mathbf{w}_{20}(1) + \mathbf{w}_{22}(1) \\ -\left(\mathbf{w}_{20}(1) + \frac{1}{2}\mathbf{w}_{22}(1)\right)M & -2\mathbf{w}_{20}(1) - \mathbf{w}_{22}(1) \end{pmatrix}\mathbf{w}_{20}$$

$$- \frac{1}{2}\gamma\begin{pmatrix} \left(\mathbf{w}_{20}(1) + \mathbf{w}_{22}(1)\right)M & 2\left(\mathbf{w}_{20}(1) + \mathbf{w}_{22}(1)\right) \\ -\left(\mathbf{w}_{20}(1) + \mathbf{w}_{22}(1)\right)M & -2\left(\mathbf{w}_{20}(1)+\mathbf{w}_{22}(1)\right) \end{pmatrix}\mathbf{w}_{22},$$

$$\mathbf{P}_3^{(3)} = \begin{pmatrix} 0 & 0 \\ 0 & 9d^{(2)}k_c^2 \end{pmatrix}\mathbf{w}_{33} - \frac{1}{2}\gamma\begin{pmatrix} \frac{2b}{(a+b)^2} + 2(a+b)M & 2(a+b) \\ -\frac{2b}{(a+b)^2} - 2(a+b)M & -2(a+b) \end{pmatrix}\mathbf{w}_{42}$$

$$- \gamma\begin{pmatrix} \frac{2b}{(a+b)^2}\mathbf{w}_{20}(1) + 2(a+b)\mathbf{w}_{20}(2) & 2(a+b)\mathbf{w}_{20}(1) + \frac{1}{2} \\ -\frac{2b}{(a+b)^2}\mathbf{w}_{20}(1) - 2(a+b)\mathbf{w}_{20}(2) & -2(a+b)\mathbf{w}_{20}(1) - \frac{1}{2} \end{pmatrix}\mathbf{w}_{31},$$

$$\mathbf{P}_3^{(5)} = -\frac{1}{2}\gamma \begin{pmatrix} \frac{2b}{(a+b)^2} + 2(a+b)M & 2(a+b) \\ -\frac{2b}{(a+b)^2} - 2(a+b)M & -2(a+b) \end{pmatrix} (\mathbf{w}_{43} + \mathbf{w}_{44})$$

$$-\gamma \begin{pmatrix} \frac{2b}{(a+b)^2}\mathbf{w}_{20}(1) + 2(a+b)\mathbf{w}_{20}(2) & 2(a+b)\mathbf{w}_{20}(1) + \frac{1}{2} \\ -\frac{2b}{(a+b)^2}\mathbf{w}_{20}(1) - 2(a+b)\mathbf{w}_{20}(2) & -2(a+b)\mathbf{w}_{20}(1) - \frac{1}{2} \end{pmatrix} \mathbf{w}_{33}$$

$$-\frac{1}{2}\gamma \begin{pmatrix} \frac{2b}{(a+b)^2}\mathbf{w}_{20}(1) + 2(a+b)\mathbf{w}_{20}(2) & 2(a+b)\mathbf{w}_{20}(1) + \frac{1}{2} \\ -\frac{2b}{(a+b)^2}\mathbf{w}_{20}(1) - 2(a+b)\mathbf{w}_{20}(2) & -2(a+b)\mathbf{w}_{20}(1) - \frac{1}{2} \end{pmatrix} \mathbf{w}_{32}$$

$$-\frac{1}{2}\gamma \begin{pmatrix} M\mathbf{w}_{20}(1) & 2\mathbf{w}_{20}(1) \\ -M\mathbf{w}_{20}(1) & -2\mathbf{w}_{20}(1) \end{pmatrix} \mathbf{w}_{22}$$

$$-\frac{1}{2}\gamma \begin{pmatrix} M\mathbf{w}_{22}(1) & 2\mathbf{w}_{22}(1) \\ -M\mathbf{w}_{22}(1) & -2\mathbf{w}_{22}(1) \end{pmatrix} \left(\mathbf{w}_{20} + \frac{1}{2}\mathbf{w}_{22} \right),$$

$$\mathbf{P}_5^{(5)} = -\frac{1}{2}\gamma \begin{pmatrix} \frac{2b}{(a+b)^2} + 2(a+b)M & 2(a+b) \\ -\frac{2b}{(a+b)^2} - 2(a+b)M & -2(a+b) \end{pmatrix} \mathbf{w}_{44}$$

$$-\frac{1}{2}\gamma \begin{pmatrix} \frac{2b}{(a+b)^2}\mathbf{w}_{20}(1) + 2(a+b)\mathbf{w}_{20}(2) & 2(a+b)\mathbf{w}_{20}(1) + \frac{1}{2} \\ -\frac{2b}{(a+b)^2}\mathbf{w}_{20}(1) - 2(a+b)\mathbf{w}_{20}(2) & -2(a+b)\mathbf{w}_{20}(1) - \frac{1}{2} \end{pmatrix} \mathbf{w}_{33}$$

$$-\frac{1}{4}\gamma \begin{pmatrix} M\mathbf{w}_{22}(1) & 2\mathbf{w}_{22}(1) \\ -M\mathbf{w}_{22}(1) & -2\mathbf{w}_{22}(1) \end{pmatrix} \mathbf{w}_{22}.$$

Putting:

$$\tilde{\sigma} = -\frac{\left\langle \mathbf{P}_1^{(1)}, \boldsymbol{\psi} \right\rangle}{\langle \mathbf{r}, \boldsymbol{\psi} \rangle}, \qquad L = \frac{\left\langle 3\sigma\mathbf{w}_{32} - L\mathbf{w}_{31} + \mathbf{P}_1^{(3)}, \boldsymbol{\psi} \right\rangle}{\langle \mathbf{r}, \boldsymbol{\psi} \rangle},$$

$$R = \frac{\left\langle 3L\mathbf{w}_{32} + \mathbf{P}_1^{(5)}, \boldsymbol{\psi} \right\rangle}{\langle \mathbf{r}, \boldsymbol{\psi} \rangle} \tag{32}$$

the Fredholm alternative $\langle \mathbf{P}, \boldsymbol{\psi} \rangle$ for the Eq. (31) leads to:

$$\frac{\partial A}{\partial T_4} = \tilde{\sigma} A - \tilde{L} A^3 + \tilde{R} A^5. \tag{33}$$

Adding up (33) to (24) one gets (26), with:

$$\bar{\sigma} = \sigma + \varepsilon^2 \tilde{\sigma}, \qquad \bar{L} = L + \varepsilon^2 \tilde{L}, \qquad \bar{R} = \varepsilon^2 \tilde{R}. \tag{34}$$

References

1. Aragon, J., Barrio, R., Woolley, T., Baker, R., Maini, P.: Nonlinear effects on Turing patterns: time oscillations and chaos. Phys. Rev. E **86**(2), 026201 (2012). doi:10.1103/PhysRevE.86.026201
2. Atis, S., Saha, S., Auradou, H., Salin, D., Talon, L.: Autocatalytic reaction fronts inside a porous medium of glass spheres. Phys. Rev. Lett. **110**(14), 148301 (2013)
3. Barbera, E., Consolo, G., Valenti, G.: Spread of infectious diseases in a hyperbolic reaction-diffusion susceptible-infected-removed model. Phys. Rev. E **88**(5), 052719 (2013)
4. Barreira, R., Elliott, C.M., Madzvamuse, A.: The surface finite element method for pattern formation on evolving biological surfaces. J. Math. Biol. **63**(6), 1095–1119 (2011)
5. Bilotta, E., Pantano, P.: Emergent patterning phenomena in $2D$ cellular automata. Artif. Life **11**(3), 339–362 (2005)
6. Bilotta, E., Pantano, P., Stranges, F.: A gallery of Chua attractors: part II. Int. J. Bifurcat. Chaos **17**(02), 293–380 (2007)
7. Bozzini, B., Gambino, G., Lacitignola, D., Lupo, S., Sammartino, M., Sgura, I.: Weakly nonlinear analysis of Turing patterns in a morphochemical model for metal growth. Comput. Math. Appl. **70**, 1948–1969 (2015)
8. Cangelosi, R., Wollkind, D., Kealy-Dichone, B., Chaiya, I.: Nonlinear stability analysis of Turing patterns for a mussel-algae model. J. Math. Biol. 1–46 (2014)
9. Capone, F., De Luca, R., Rionero, S.: On the stability of non-autonomous perturbed Lotka-Volterra models. Appl. Math. Comput. **219**(12), 6868–6881 (2013)
10. Chattopadhyay, J., Tapaswi, P.: Effect of cross-diffusion on pattern formation—a nonlinear analysis. Acta Appl. Math. **48**, 1–12 (1997)
11. Galiano, G., Selgas, V.: On a cross-diffusion segregation problem arising from a model of interacting particles. Nonlinear Anal. Real World Appl. **18**, 34–49 (2014)
12. Galiano, G., Velasco, J.: Finite element approximation of a surface-subsurface coupled problem arising in forest dynamics. Math. Comput. Simul. **102**, 62–75 (2014)
13. Gambino, G., Lombardo, M., Sammartino, M.: Global linear feedback control for the generalized Lorenz system. Chaos Solitons Fractals **29**(4), 829–837 (2006)
14. Gambino, G., Lombardo, M., Sammartino, M.: Adaptive control of a seven mode truncation of the Kolmogorov flow with drag. Chaos Solitons Fractals **41**(1), 47–59 (2009)
15. Gambino, G., Lombardo, M., Sammartino, M.: Pattern formation driven by cross-diffusion in a 2D domain. Nonlinear Anal. Real World Appl. **14**(3), 1755–1779 (2013)
16. Gambino, G., Lombardo, M., Sammartino, M.: Turing instability and pattern formation for the Lengyel–Epstein system with nonlinear diffusion. Acta Appl. Math. 1–12 (2014)
17. Gambino, G., Lombardo, M.C., Sammartino, M.: Turing instability and traveling fronts for a nonlinear reaction-diffusion system with cross-diffusion. Math. Comput. Simul. **82**(6), 1112–1132 (2012)
18. Gambino, G., Lombardo, M.C., Sammartino, M., Sciacca, V.: Turing pattern formation in the Brusselator system with nonlinear diffusion. Phys. Rev. E **88**, 042–925 (2013)
19. Gambino, G., Sciacca, V.: Intermittent and passivity based control strategies for a hyperchaotic system. Appl. Math. Comput. **221**, 367–382 (2013)
20. Ghergu, M., Radulescu, V.: Turing patterns in general reaction-diffusion systems of Brusselator type. Commun. Contemp. Math. **12**(04), 661–679 (2010)
21. Kolokolnikov, T., Erneux, T., Wei, J.: Mesa-type patterns in the one-dimensional Brusselator and their stability. Physica D **214**(1), 63–77 (2006)
22. Kolokolnikov, T., Ward, M., Wei, J.: Self-replication of mesa patterns in reaction-diffusion systems. Phys. D **236**(2), 104–122 (2007)
23. Lacitignola, D., Bozzini, B., Sgura, I.: Spatio-temporal organization in a morphochemical electrodeposition model: Hopf and Turing instabilities and their interplay. Eur. J. Appl. Math. **26**(2), 143–173 (2015)
24. Lin, Z., Ruiz-Baier, R., Tian, C.: Finite volume element approximation of an inhomogeneous Brusselator model with cross-diffusion. J. Comput. Phys. **256**, 806–823 (2014)
25. Madzvamuse, A., Ndakwo, H., Barreira, R.: Cross-diffusion-driven instability for reaction-diffusion systems: analysis and simulations. J. Math. Biol. **70**(4), 709–743 (2015)
26. Medina, V., Champneys, A.: Subcritical Turing bifurcation and the morphogenesis of localized patterns. Phys. Rev. E **90**, 032,923–1–6 (2014)

27. Mulone, G., Rionero, S., Wang, W.: The effect of density-dependent dispersal on the stability of populations. Nonlinear Anal. **74**(14), 4831–4846 (2011)
28. Mulone, G., Straughan, B.: Nonlinear stability for diffusion models in biology. SIAM J. Appl. Math. **69**(6), 1739–1758 (2009)
29. Rionero, S.: L^2-energy decay of convective nonlinear PDEs reaction-diffusion systems via auxiliary ODEs systems. Ricerche di Matematica **64**(2), 251–287 (2015)
30. Ruiz-Baier, R., Tian, C.: Mathematical analysis and numerical simulation of pattern formation under cross-diffusion. Nonlinear Anal. Real World Appl. **14**(1), 601–612 (2013)
31. Satulovsky, J.: Lattice Lotka–Volterra models and negative cross-diffusion. J. Theor. Biol. **183**, 381–389 (1996)
32. Tian, C., Lin, Z., Pedersen, M.: Instability induced by cross-diffusion in reaction-diffusion systems. Nonlinear Anal. Real World Appl. **11**(2), 1036–1045 (2010)
33. Tian, C., Ling, Z., Lin, Z.: Spatial patterns created by cross-diffusion for a three-species food chain model. Int. J. Biomath **07**(02), 1450,013 (2014)
34. Tulumello, E., Lombardo, M., Sammartino, M.: Cross-diffusion driven instability in a predator-prey with cross-diffusion. Acta Appl. Math. **132**, 621–633 (2014)
35. Vanag, V., Epstein, I.: Cross-diffusion and pattern formation in reaction-diffusion systems. Phys. Chem. Chem. Phys. 897–912 (2009)
36. Vilas, C., Garcia, M., Banga, J., Alonso, A.: Robust feed-back control of travelling waves in a class of reaction-diffusion distributed biological systems. Phys. D **237**(18), 2353–2364 (2008)
37. Yi, F., Wei, J., Shi, J.: Diffusion-driven instability and bifurcation in the Lengyel–Epstein system. Nonlinear Anal. Real World Appl. **9**(3), 1038–1051 (2008)
38. Zemskov, E.P., Kassner, K., Hauser, M.J.B., Horsthemke, W.: Turing space in reaction-diffusion systems with density-dependent cross diffusion. Phys. Rev. E **87**, 032,906 (2013)